International Journal of Fluid Mechanics & Thermal Sciences
2021; 7(4): 53-67
http://www.sciencepublishinggroup.com/j/ijfmts
doi: 10.11648/j.ijfmts.20210704.11
ISSN: 2469-8105 (Print); ISSN: 2469-8113 (Online)

Numerical Simulation of the Velocity Fields Generated by a Plume in Enclosure with Several Openings

Kouéni Toko Christian Anicet

Department of Renewable Energy, Ecole Nationale Superieure Polytechnique de Maroua, University of Maroua, Maroua, Cameroon

Email address:
christiandrkoueni@gmail.com

To cite this article:
Kouéni Toko Christian Anicet. Numerical Simulation of the Velocity Fields Generated by a Plume in Enclosure with Several Openings. *International Journal of Fluid Mechanics & Thermal Sciences*. Vol. 7, No. 4, 2021, pp. 53-67. doi: 10.11648/j.ijfmts.20210704.11

Received: February 12, 2022; **Accepted**: February 28, 2022; **Published**: March 3, 2022

Abstract: The objective of this study is to understand and control the phenomena generated by a plume in a semi-ventilated enclosure using velocity fields. The enclosure has a rectangular cross-section and twenty openings located near the floor on two side walls. Each side wall has ten openings distributed over two horizontal rows on the axis (0y) in equal number. The plume is created by a linear source. The study is carried out in a steady state. To solve the mass and momentum conservation equations, the Direct Numerical Simulation (DNS) method and the finite volume method were used to discretize the differential equations. The fine non-uniform regular mesh was chosen to reduce calculation errors, to have a rapid convergence of the conservations equations and a stable result which approaches reality. As discretization scheme, we used the QUICK scheme and schema "Body Strength weighted for the resolution of the pressure. We have shown the influence of the reduced Grashof number on the fields of mean velocity, velocity along the (0z) w axis, velocity along the (0x) u axis and on the differential static pressure profiles. We compared the dimensionless differential static pressure results against the relevant experimental and the numerical calculations results. The results obtained showed that the velocity plume w can take the positions centered, tilted to the left and tilted to the right in the enclosure according to the increase in the number of reduced Grashof The velocity plume w reaches the ceiling where it is destroyed and go back down to the bottom of the enclosure. The maximum absolute values of the velocity w in the plume and u at the openings increase with the increase in the reduced Grashof number. The neutral height has for value $z+=0.05$. At the openings, cool air enters the enclosure through openings near the floor and below neutral height, and hot air exits through openings above neutral height. The comparison of the dimensionless differential static pressure results with against the relevant experimental and numerical calculations results is concordant.

Keywords: Enclosure, Openings, Plume, Velocity Fields, Numerical Computation

1. Introduction

A thermal or dynamic plume is a mass of air distinguished from the surrounding air by a temperature, a speed, a density and a very different composition and evolving according to its momentum, the diffusion of matter and buoyancy [1, 2]. This can apply to the phenomena of a plume of smoke coming out of a chimney, a fire in a room or in the open air, a plume of hot air in a room or in the open air, etc. Therefore a plume can be created both in confined [3, 4], semi-ventilated [5–7] and ventilated [8–13] than in the open air by a distributed or linear or point heat source.

We will focus in this study on the plume created by a heat source in a semi-ventilated or ventilated enclosure. Concerning this study, several works were carried out in particular those of Linden, Lane-Serff and Smeed [11], who studied the case of a point source of buoyancy placed in an enclosure having two openings, height H and radius R, with an aspect ratio H/R < 1. They showed that there is a displacement regime and that stratification developed characterized by two layers separated by an interface. Kaye and Hunt [12], studied the same type of situation in the case of a rectangular enclosure presenting a heat source located at the bottom of the enclosure and two openings located at the base and at the top. They have shown that the steady state depends the filling time and the emptying time. For aspect ratios of 1 <H/R <5.8, Kaye and Hunt [14], have shown that the windings appear near the walls and induce an additional

training of air which has the effect of thickening the top layer (uniform temperature layer). In the same situation, Koueni Toko [6] studied experimentally, analytically and numerically, the temperature in an enclosure semi - ventilated, heated by a linear heat source (case 11). He showed that, when a constant temperature ΔT_0 is imposed at the heat source and in a steady state, the thermal plume in the enclosure was symmetrical and that at each opening, an entry of fresh air is observed near the floor and a hot gas outlet at the top. Therefore, the neutral height is less than the height of the openings. According to Karl Terpager A. [15], the neutral plane is the plane for which the static pressure inside the enclosure is equal to the pressure outside. Koueni *et al*. [7] studied Numerical modeling of the temperature fields in a semi-confined enclosure heated by a linear heat source. The enclosure has an aspect ratio H/L=2.476 and twenty openings located near the floor on two side walls of height H and width l. Each side wall has ten openings distributed over two horizontal rows on the axis (0y) in equal number. The heat source is linear. They showed in steady state that the thermal plume was near-centered and the temperature values in the enclosure increased as the reduced Rayleigh number increased.

We will study in this paper a numerical simulation of the velocity fields generated by a plume in enclosure with several openings. The enclosure configuration is identical to those of Koueni *et al.* [7].

The objective of this study is to understand and control the phenomena generated by a plume in a semi-ventilated enclosure using velocity fields. We will show in this study the influence of the reduced Grashof number on the fields of average velocity, of velocity along the (0z) w axis, of velocity along the (0x) u axis and on the differential static pressure profiles. Then we compared the dimensionless differential static pressure results with the experimental results and numerical calculations of case 11 of Koueni Toko [6].

2. Numerical Device

This device is of a rectangular enclosure, with a square base of side *l=L=210 mm* and height *H=520 mm*. Its side walls of identical sections (210×520 mm^2) are of Plexiglas 8mm thick. The floor and ceiling of the enclosure also are identical sections (210×210 mm^2) made of Plexiglas 14mm thick. These walls are connected together by fitting connections and assembled with glue.

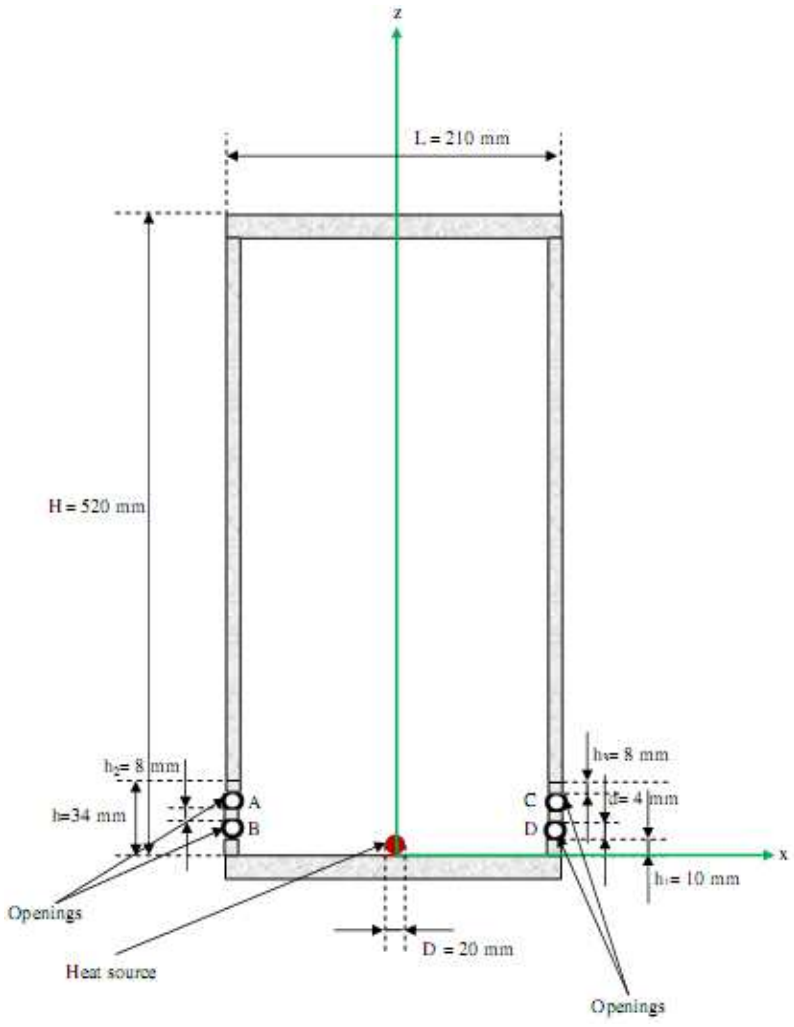

Figure 1. *Numerical device, front view [7].*

As shown in Figure 1, this enclosure communication with the outside through various openings. These openings have same sections: height $h=4$ *mm*, width $l=4$ *mm* and are located on the two opposite side walls of weaker sections relative to the linear heat source. The number of openings on each of the walls is twenty.

The geometrical characteristics, as well as the material of the numerical device are same to numerical device of Koueni *et al.* [7]. These characteristics are shown in Table 2.

On Figure 1, appears a coordinate system. Point O is the center of the axis system. The Ox axis is the x-axis, the Oy axis is the y-axis and the Oz axis is anz-axis perpendicular to the plane formed by Ox and Oy. The coordinates of the points are (x, y and z).

The enclosure is heated by a linear and cylindrical source of diameter $D_0=20$ *mm* and length $l_0=200$ *mm*located near the floor at$x=0$ and parallel to the axis Oy. Before switching on the heating system, the enclosure is in equilibrium with the external environment. The outer surfaces of walls of the enclosure, except the floor, are in contact with the outside air. The outer surface of the floor is at the temperature of the metal table on which rests the enclosure. As the boundary conditions to the walls of the enclosure, we have the convective condition on all the walls of the enclosure except the floor where we imposed a Dirichlet condition.

The temperature of the heating source is fixed in value $\Delta T_0=T_0 - T_{ext}$. T_0 is the temperature of the thermocouple placed in the heat source and T_{ext} is the temperature outside the enclosure. Three values of ΔT_0 as 40, 60, and 75 K were used for this study.

To model our device, we opted for a cylindrical heat source with a square base section. The sections of the openings have square shapes.

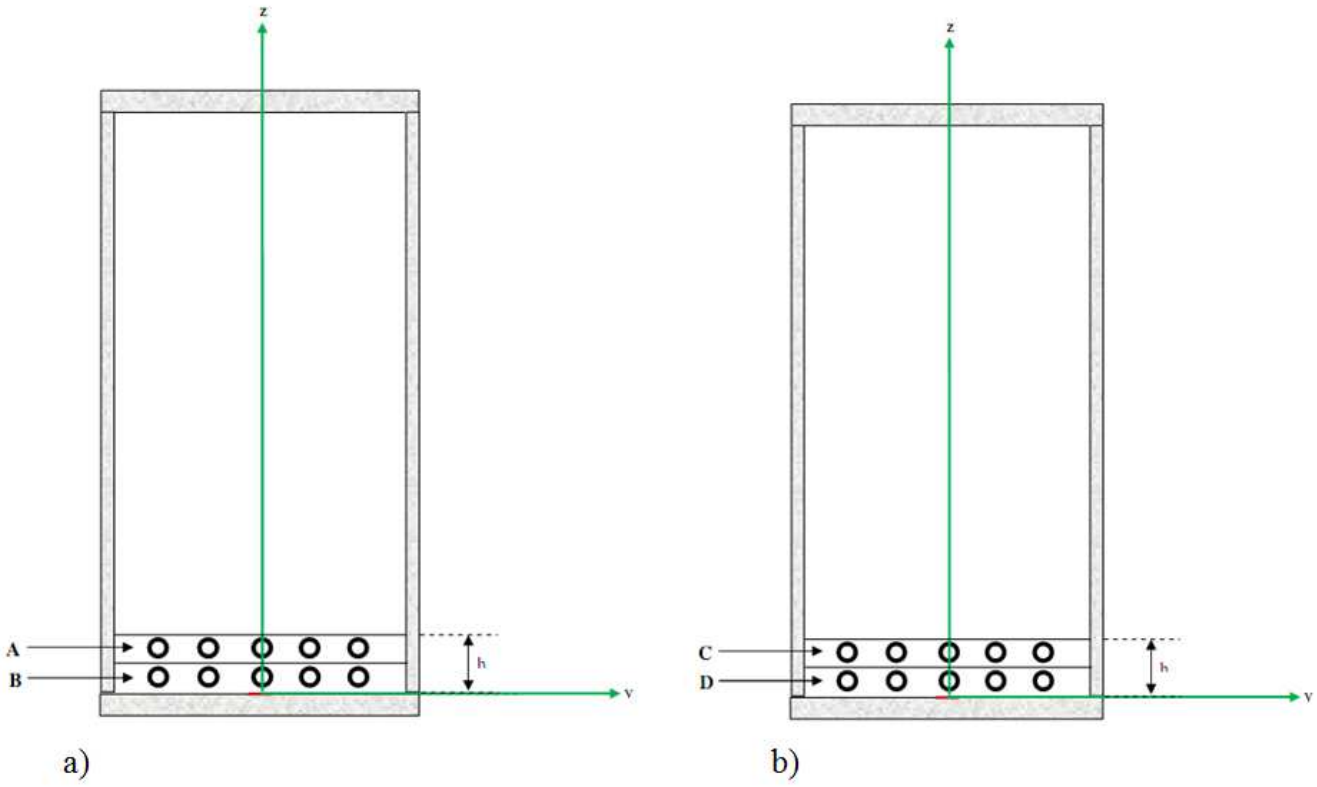

Figure 2. *Numerical device, a) left wall b) right wall [7].*

Table 1. *Values of theGrashof numbers reduced depending ΔT_0.*

ΔT_0 (K)	40	60	75
Gr*	2.10×10^9	3.47×10^9	4.42×10^9

Table 2. *Characteristics of Numerical devise meshes.*

Meshes	Mesh 1	Mesh 2	Mesh 3
Cells	89001	366654	1122786
Nodes	95812	384048	1230921

3. Mathematical and Numerical Formulation Procedure

3.1. Mathematical Formulation

To establish the mathematical and representative model of the physical problem of our study, we started from the mass and momentum conservation equations for a viscous compressible fluid. We considered that the velocity plume is

turbulent and that the local derivatives of the density ($\frac{\partial \rho}{\partial t}$) and velocity ($\frac{\partial u}{\partial t}, \frac{\partial v}{\partial t}, \frac{\partial w}{\partial t}$) are zero. And that convection is natural. We put ourselves in the same conditions as Kouéni Toko [6] for the measurements of static pressure differentials which are carried out in calm weather (calm air). The temperature of the heat source is constant over time. Heat transfer by radiation is negligible. The physical properties of the fluid are constant except for the density obeying the Boussinesq's approximation in terms of the buoyancy, and the dissipated power density is negligible. The density of the air in the enclosure is a function of the temperature according to equation (1).

$$\rho = \rho(T) \tag{1}$$

The mass equationis given by equation (2):

$$\rho\left(\frac{\partial u}{\partial x} + \frac{\partial v}{\partial y} + \frac{\partial w}{\partial z}\right) = 0 \tag{2}$$

u, v et w are the components of the velocity in the x, y and z respectively.

According to Morton *et al.* [1], the Buoyancyis given by equation (3).

$$\frac{\rho_0 - \rho}{\rho_1} = \beta(T - T_0) \tag{3}$$

With

ρ_1: Reference density;

ρ_0: Outside density of enclosure;

T_0: Outside temperature of enclosure.

For a gas, β is given by the expression (4)

$$\beta \sim \frac{1}{T_1} \tag{4}$$

T_1: Reference temperature.

According to Kouéni Toko [6], the Buoyancy force generated by the heat is given by:

$$g\beta(T - T_{ext}).$$

With

T: The inside local temperature of enclosure.

The heat source is a heating cylinder which is a solid. This heating cylinder at a time constant. When the heating cylinder is energized in the semi - ventilated enclosure, its temperature gradually increases until it reaches the value ΔT_0 then a thermal regulation system maintains ΔT_0 at a constant value. From switching on the heating system to the regulation temperature, the temperature ΔT_0 varies over time from the value 0 to the value 40 or 60 or 75 K [6]. According to Koueni Toko [6], as soon as the heating system is started in the semi - ventilated enclosure of aspect ratio 2.476, for $\Delta T_0 < 5K$, air movement is observed in the enclosure and at the openings. Following this situation, we considered Boussinesq's approximation for the mathematical formulation of our problem. Which implies $|\delta\rho| \ll \rho_0$ ($\frac{\rho_0}{\rho} \approx 1$).

The momentum conservation equations along the axes x, y and z, using the Boussinesq's approximation and assuming that:

$$\frac{\rho_0}{\rho} \approx 1$$

is represented as the equation 6.

Where

P_0: Pressure outside of the enclosure;

$\rho_0 = 1{,}2\ kg.m^{-3}$: Density of air outside the enclosure; It has been determined for a reference temperature of 300K;

P': Pressure at the interior in the enclosure;

ρ: Density of the air inside the enclosure.

To restrict the flow settings to make the general solution, we will use the dimensionless conservation equations set out above. The fields and profiles of pressure static differential will be presentedin dimensionless form taking into account the grandeurs without dimension [4] following:

$$x^+ = \frac{x}{L}, y^+ = \frac{y}{L}, z^+ = \frac{z}{H}, u^+ = \frac{u}{U_0}, v^+ = \frac{v}{U_0}, w^+ = \frac{w}{U_0} \text{ et } P^+ = \frac{P}{|P_{max}|}$$

With

$$U_0 = \sqrt{\frac{|P_{max}|}{\rho_\infty}} \tag{5}$$

The maximum velocity air inlet cool into the enclosure when the heat source is at a temperature ΔT_0.

$\delta = \frac{\mathrm{L}}{\mathrm{H}} = \frac{1}{2{,}476}$: The inverse of aspect ratio;

$Gr = \frac{g\beta H^3(T_0 - T_{ext})}{\nu^2}$: The Grashof number;

$Gr^* = \delta^2 Gr$: The Grashof number reduced;

$Pr = \frac{\nu}{\alpha}$: The Prandtl number.

$$\begin{cases} u\frac{\partial u}{\partial x} + v\frac{\partial u}{\partial y} + w\frac{\partial u}{\partial z} = -\frac{1}{\rho}\frac{\partial P}{\partial x} + \nu\left(\frac{\partial^2 u}{\partial x^2} + \frac{\partial^2 u}{\partial y^2} + \frac{\partial^2 u}{\partial z^2}\right) \\ u\frac{\partial v}{\partial x} + v\frac{\partial v}{\partial y} + w\frac{\partial v}{\partial z} = -\frac{1}{\rho}\frac{\partial P}{\partial y} + \nu\left(\frac{\partial^2 v}{\partial x^2} + \frac{\partial^2 v}{\partial y^2} + \frac{\partial^2 v}{\partial z^2}\right) \\ u\frac{\partial w}{\partial x} + v\frac{\partial w}{\partial y} + w\frac{\partial w}{\partial z} = -\frac{1}{\rho}\frac{\partial P}{\partial z} + \nu\left(\frac{\partial^2 w}{\partial x^2} + \frac{\partial^2 w}{\partial y^2} + \frac{\partial^2 w}{\partial z^2}\right) - g\beta(T - T_{ext}) \end{cases} \tag{6}$$

With

$$\frac{\partial P}{\partial z} = \frac{\partial(P' - P_0)}{\partial z}, P_0 = P_{0i} - \rho_0 gz, P' = P'_i - \rho gz, \frac{\partial P_0}{\partial z} = -\rho_0 gz, \frac{\partial P'}{\partial z} = -\rho gz, \frac{\partial(P' - P_0)}{\partial z} = (\rho_0 - \rho) \tag{7}$$

The momentum conservation equations of dimensionless [6] along the axes x+, y+ and z+ are represented by a system 8:

$$\begin{cases} \frac{u^+}{\delta}\frac{\partial u^+}{\partial x^+}+\frac{v^+}{\delta}\frac{\partial u^+}{\partial y^+}+w^+\frac{\partial u^+}{\partial z^+}=-\frac{1}{\delta}\frac{\partial P^+}{\partial x^+}+\frac{1}{Gr^{*1/2}}\left(\frac{\partial^2 u^+}{\partial x^{+2}}+\frac{\partial^2 u^+}{\partial y^{+2}}+\delta\frac{\partial^2 u^+}{\partial z^{+2}}\right) \\ \frac{u^+}{\delta}\frac{\partial v^+}{\partial x^+}+\frac{v^+}{\delta}\frac{\partial v^+}{\partial y^+}+w^+\frac{\partial v^+}{\partial z^+}=-\frac{1}{\delta}\frac{\partial P^+}{\partial y^+}+\frac{1}{Gr^{*1/2}}\left(\frac{\partial^2 v^+}{\partial x^{+2}}+\frac{\partial^2 v^+}{\partial y^{+2}}+\delta\frac{\partial^2 v^+}{\partial z^{+2}}\right) \\ \frac{u^+}{\delta}\frac{\partial w^+}{\partial x^+}+\frac{v^+}{\delta}\frac{\partial w^+}{\partial y^+}+w^+\frac{\partial w^+}{\partial z^+}=-\frac{1}{\delta}\frac{\partial P^+}{\partial z^+}+\frac{1}{Gr^{*1/2}}\left(\frac{\partial^2 w^+}{\partial x^{+2}}+\frac{\partial^2 w^+}{\partial y^{+2}}+\delta\frac{\partial^2 w^+}{\partial z^{+2}}\right)-T^+ \end{cases} \quad (8)$$

The conservation equation of dimensionless mass [6] is:

$$\rho\left(\frac{1}{\delta}\frac{\partial u^+}{\partial x^+}+\frac{1}{\delta}\frac{\partial v^+}{\partial y^+}+\frac{\partial w^+}{\partial z^+}\right)=0 \quad (9)$$

3.2. Numerical Procedure

Solving the equations of a physical phenomenon was made by the use of the direct numerical simulation (DNS) as a simulation technique. It is based on the finite volume method. We used the DNS because the thermal plume created by the heat source at temperature ΔT_0 is assumed to be turbulent. The discretization of these equations gives a system of algebraic equations whose solution allows us to determine the fields of all the variables of the problem considered. This method was developed by Patankar [16]. The DNS is a computational fluid dynamics simulation in which the Navier - Stokes equations are solved numerically without any turbulence model. This means that the full range of spatial and temporal scales of turbulence must be resolved. All the spatial scales of the turbulence must be solved in the computational mesh. I used DNS against other simulation techniques to have a representative solution to the problem. The SIMPLE algorithm developed by Spalding and Patankar was used for correction of pressure on a non–uniform mesh. As discretization scheme, we used the QUICK scheme given by Leonard [17] for solving the equations of momentum conservations. And schema "Body Strength weighted for the resolution of the pressure. Calculations were performed using FLUENT commercial calculation code. In this code, the iterative calculation is performed by the linear system resolution algorithm Gauss Seidel in conjunction with algebraic multigrid method AMD to solve the resulting system.

The final solution of the problem is obtained by doing a test on the convergence by comparing the value obtained at the current iteration to the value of the previous iteration of the kind:

$$\frac{w_i-w_{i-1}}{w_{i-1}}\leq\varepsilon \quad (10)$$

With

i: Number of iterations.

A convergence test was applied to the variables u, v and w. ε is the relative error, it characterizes the degree of precision of the final solution.

If the test is negative, we do a second update w_{i-1} takes w_i and the calculation operations start again in the initial state. If the test is positive, the results are saved and the calculation stops. For our calculations, we have given ε the value 10^{-5}.

To carry out our numerical calculations we used a laptop with maximum operating speed of CPU - 2 GHz, an Intel® Core ™ i3-5005U Processor, Ram - 4GB, x64 processor, Graphics card - Intel HD Graphics 5500 (300 - 850MHz), Number of transistors - 1300 million. The CPU time is 60 s.

In this study, we will consider the conduction in the walls, consequently, the walls are not adiabatic.

To solve the equations of conservation of mass, momentum, we have meshed the numerical device. The fine non-uniformregular mesh was chosen to reduce calculation errors, to have a rapid convergence of the conservation equations and a stable result which approaches reality. Three meshes with different number of meshes (89001 meshes, 366654 meshes and 1122786 meshes) were used (Table 2) in order to determine for the resolution of the problem, the mesh which gives the optimal solution which must be independent of the density of the mesh for be sure of the realism of the solution given by the solver after convergence. This is to maintain a good Quality of the elements, to ensure a good Resolution in the regions with a strong gradient, to ensure a good Smoothing in the transition zones between the parts with fine mesh, the parts with less coarse mesh and the parts with coarse mesh; minimize the Total number of elements (reasonable computation time). From Table 4, it appears that mesh 2 of 366654 meshes is the optimal mesh which gives the optimal solution. Mesh 2 is shown in Figure 3.

The cylindrical shape with a square base section of the heat source as well as the square shape of the openings allow good smoothing, minimize distortions, have good convergence, reduce calculation time and ensure good resolution in regions with strong velocity gradients.

$$P_{total}=P_{stat}+\rho\frac{V^2}{2g}+\rho gz \quad (11)$$

$$\Delta P=P_{total,inside}-P_{total,outside} \quad (12)$$

$$S_1=L\times l \quad (13)$$

$$S_2=(H-h)\times l \quad (14)$$

Table 3. *Maximum static pressure differential values $|P_{max}|$ depending on the temperature of the heat source ΔT_0.*

ΔT_0 (K)	40	60	75
$\lvert P_{max}\rvert$(Pa) numerical device of this study	0.323	0.428	0.512
$\lvert P_{max}\rvert$(Pa) numerical device Cas 11 [6]	0.227	0.317	0.323
$\lvert P_{max}\rvert$(Pa)Experimental device Cas 11 [6]	0.16	0.24	0.3

Table 4. *Maximum static pressure differential values $|P_{max}|$ depending to the number of mesh of geometry studied for ΔT_0=40 and 75 K.*

Meshes	Mesh 1	Mesh 2	Mesh 3
$\lvert P_{max}\rvert$(Pa) ΔT_0=40 K	0.234	0.323	0.3224
$\lvert P_{max}\rvert$(Pa) ΔT_0=75 K	0.3397	0.512	0.52944

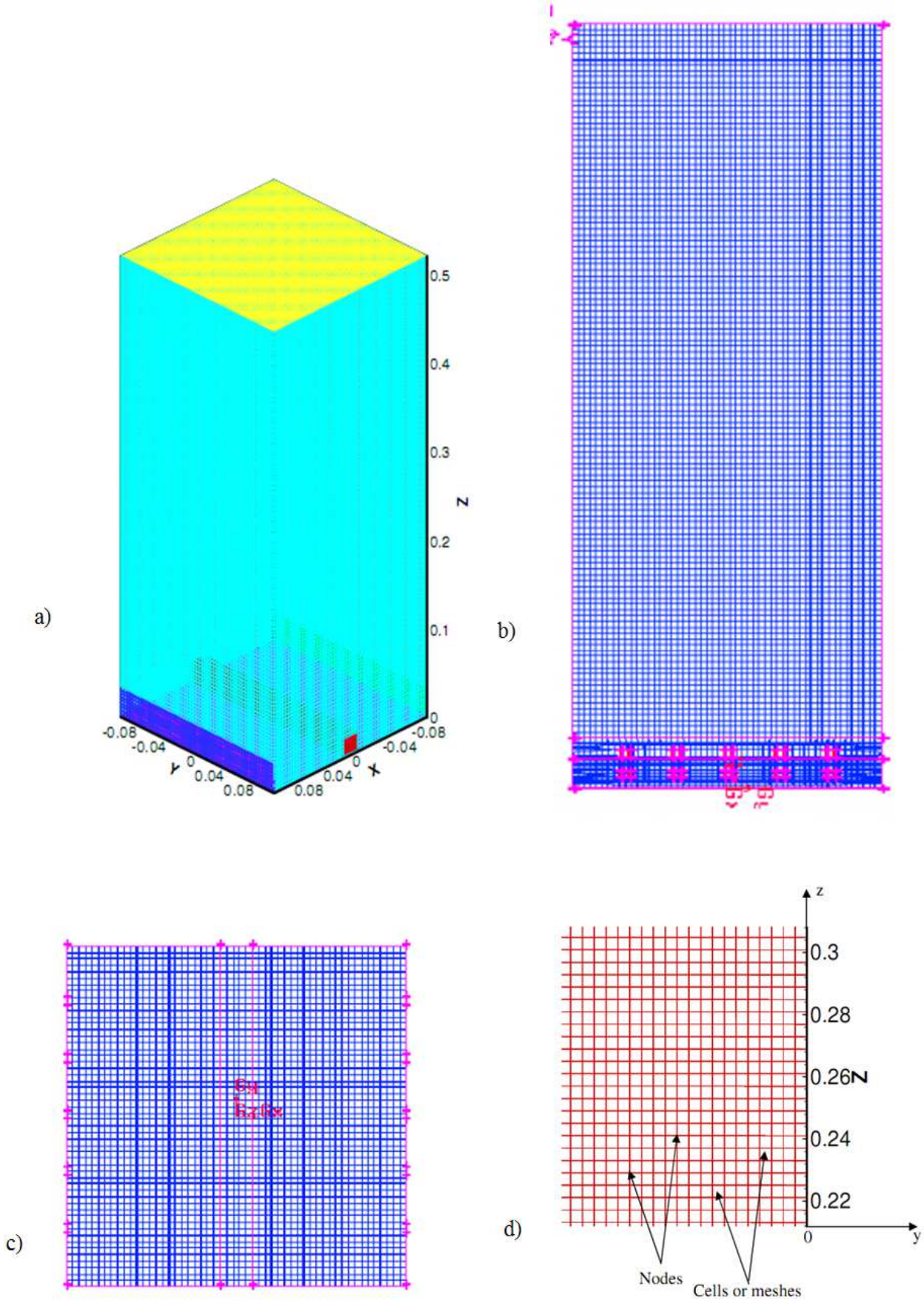

Figure 3. *Numerical mesh device a) view 3D [7], b) view 2D (z; x), c) view 2D (y; x), d) view 2D (z; y) [7].*

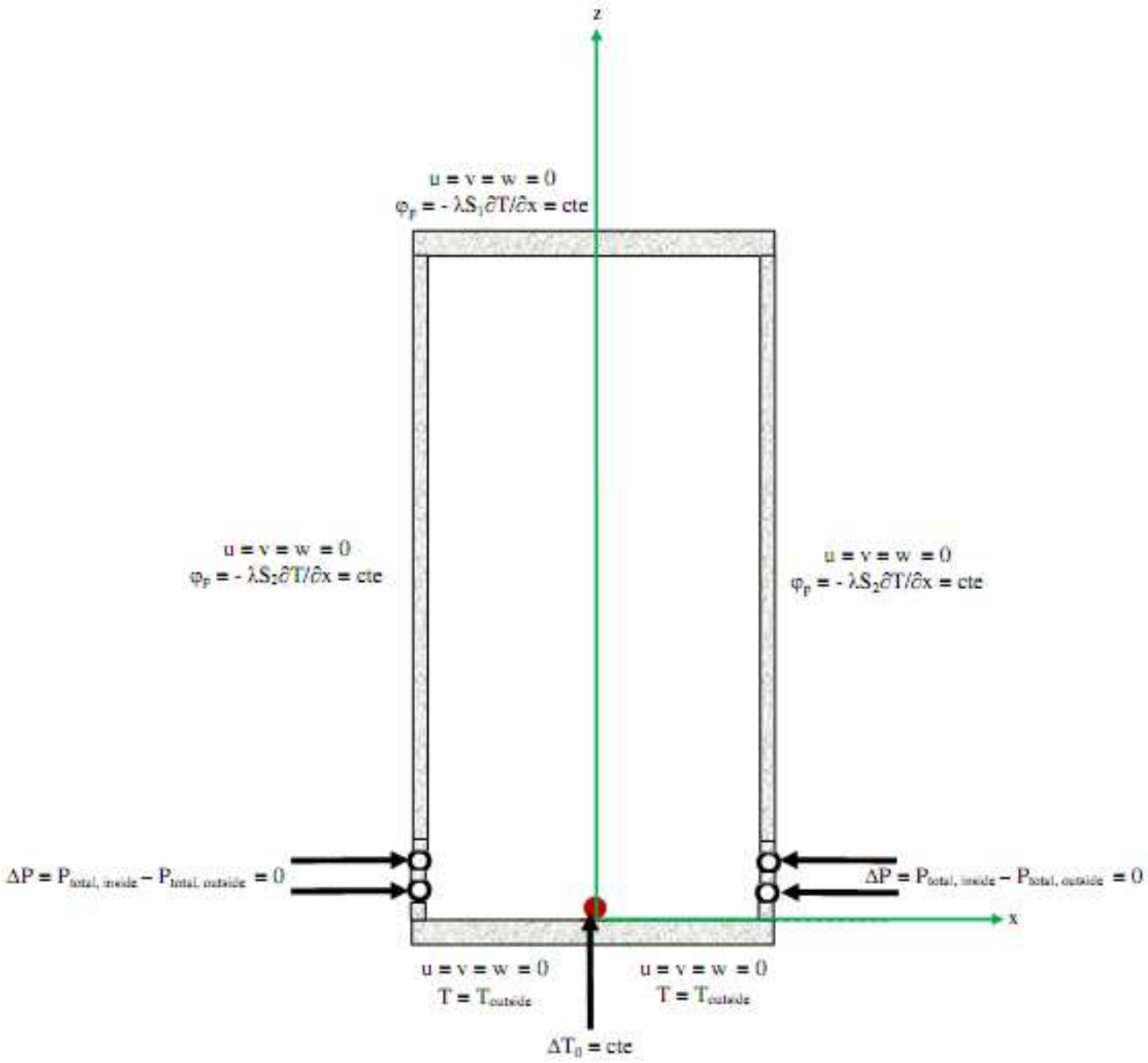

Figure 4. *Boundary condition.*

3.3. Boundary Conditions

The enclosure is placed in a large closed room with very low flux air renewal. The room is not ventilated. We put ourselves in the same experimental conditions as those of Koueni Toko [6]. Before heating begins, the enclosure is balanced with the interior of the room. Therefore, we assume that the total pressure difference (ΔP) between the inside and the outside of the enclosure is zero. There is no air entering the enclosure. The resolution of conservations equations of mass and of momentum requires the use of boundary conditions for each dependent variable. The boundary conditions of temperature, velocity and pressure to the enclosure are shown in Figure 4.

Figure 4 show that at the side walls and the ceiling we have a convective condition. That is, $\varphi_p=cte$ the heat flow which passes through each side wall and the ceiling. The expression of φ_p given by theequation (8).

$$\varphi_p = -\lambda S \frac{\partial T}{\partial x} = cte = h_i S\left(T_p - T_\infty\right) = h_o S\left(T_p - T_\infty\right) \quad (15)$$

The velocity values are zero at the walls.

4. Results and Discussion

The resultsvelocity fields and profiles and the differential static pressure profiles in function of Gr^* in the enclosure instationary state are presented in this part and discussed. The values of Gr^* in function of ΔT_0 are shown in Table 1. The values of Gr^* is greater than to 10^9. Consequently, we can consider that the thermal plume created by the heat source at

temperature ΔT_0 is turbulent.

The differential static pressure profiles obtained by numerical computations in stationary regime will be compared with Experimental measurements and numerical computations of the differential static pressure profiles have been effected by Koueni Toko [6] in stationary regime.

4.1. Influence of Grashof Reduced Number on the Velocity Magnitude Fields

Figure 5 represents the average velocity fields obtained at the position $y+=0$ and for three (03) values of the reduced Grashof number $Gr^*=2.1\times10^9$, $Gr^*=3.47\times10^9$ and $Gr^*=4.42\times10^9$. It can be seen in Figure 6a that the average velocityplume is almost centered. From the position $z+=0.6$ *to* 1, the average velocity values are almost constant in the enclosure and greater than 0 m/s. In Figure 6b, we notice that from position $z+=0$ *to* 0.3 the average velocity plume is almost centered and from position z +=0.3 to 0.6, it is tilted to the left of the enclosure. From $z+=0.6$ *to* 1, the average velocity values are almost constant in the enclosure. The medium velocity plume slopes to the right and reaches the ceiling of the enclosure and sprawls over the ceiling in Figure 6c.

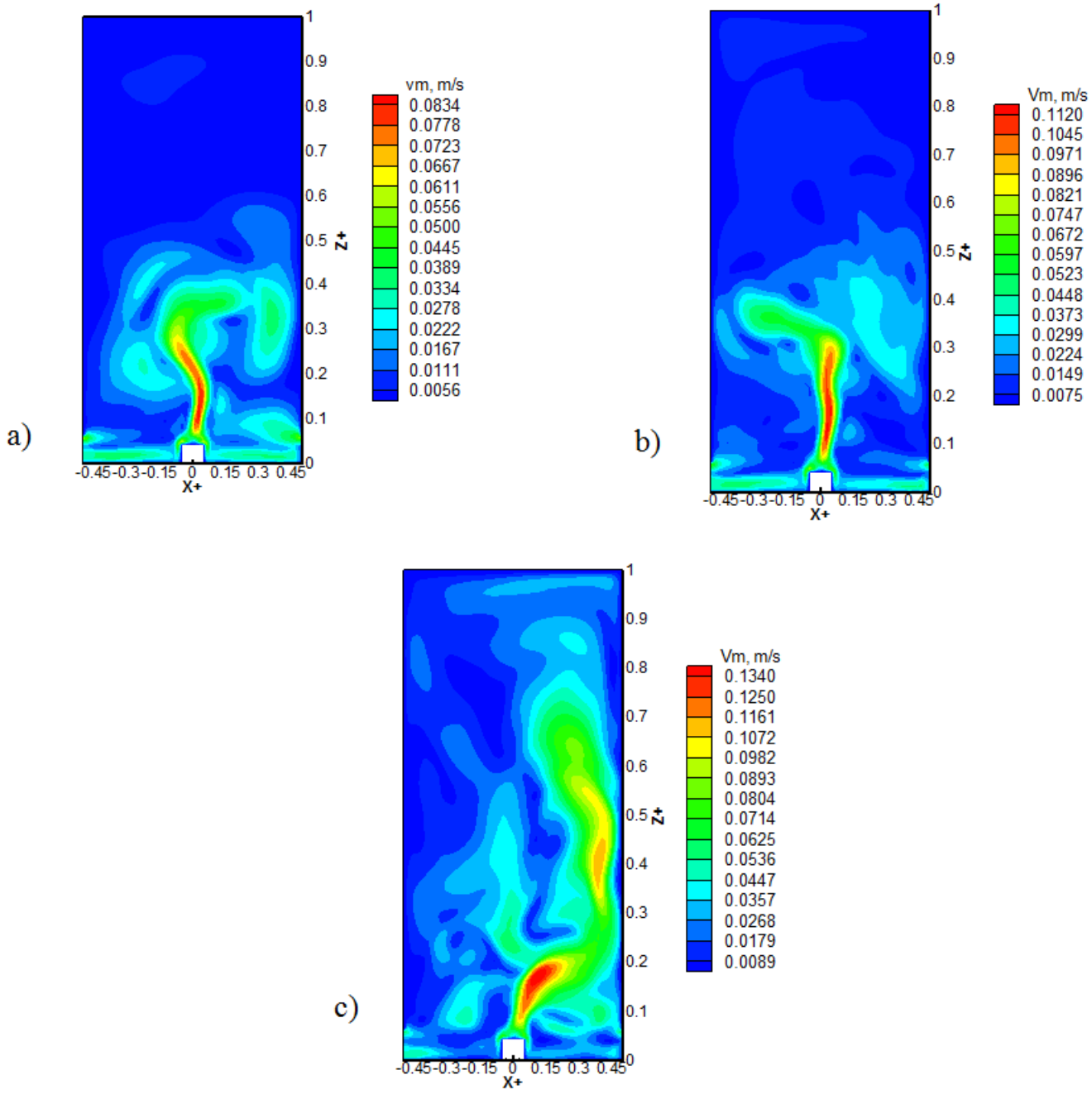

Figure 5. *Velocity magnitude fields obtained by numerical computation at $y+=0$, a) $Gr^*=2.1\times10^9$, b) $Gr^*=3.47\times10^9$, c) $Gr^*=4.42\times10^9$.*

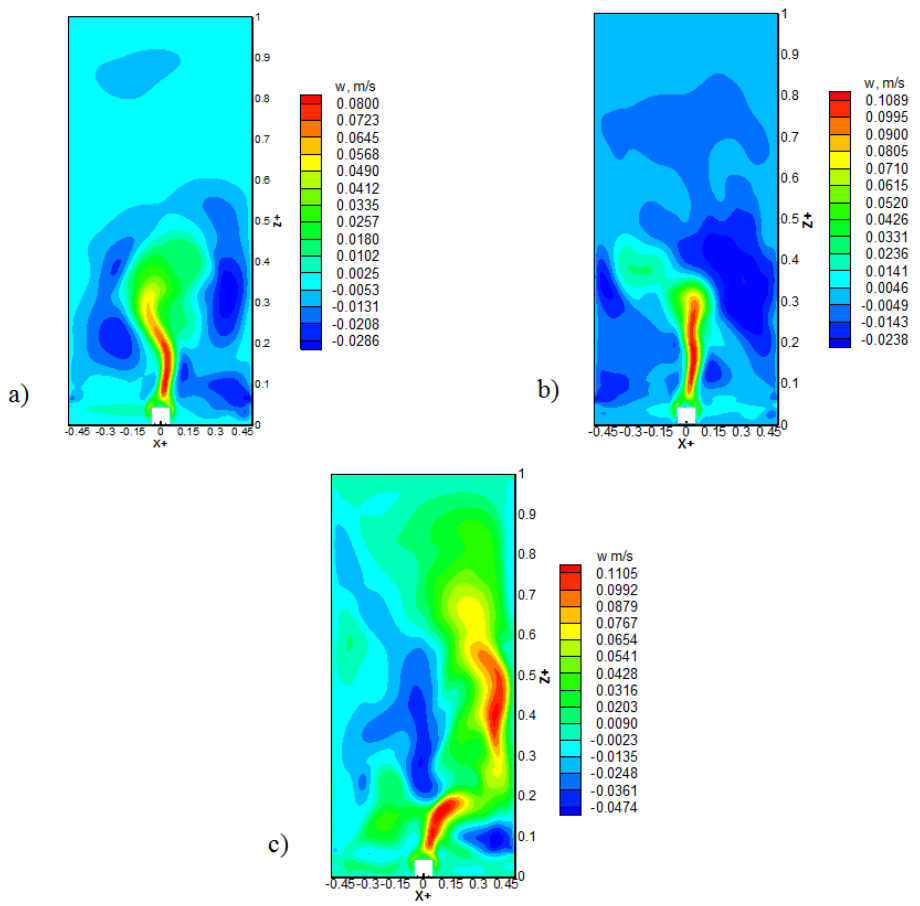

Figure 6. *z-velocity fields obtained by numerical computation at y+=0, a) Gr*=2.1×10^9, b) Gr*=3.47×10^9, c) Gr*=4.42×10^9.*

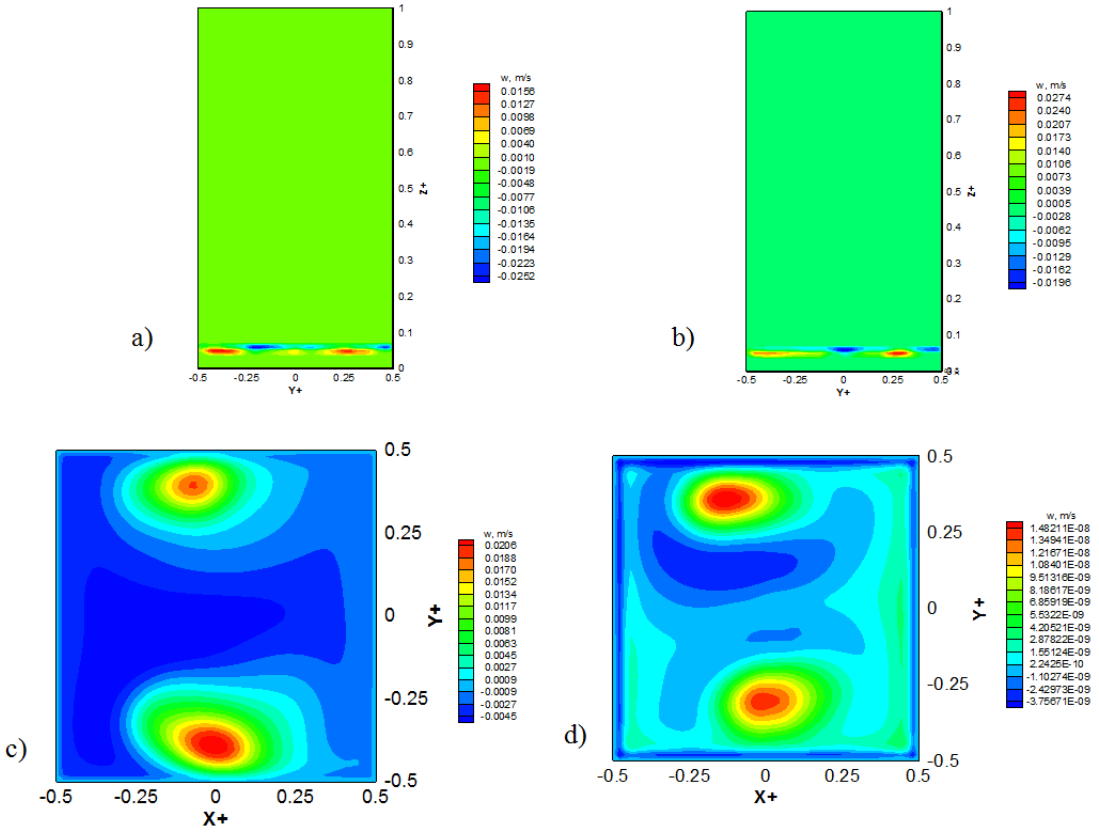

Figure 7. *z-velocity fields obtained by numerical computation at Gr*=2.1×10^9 a) x+=- 0.5, b) x+=0.5, c) z+=0.86, d) z+=1.*

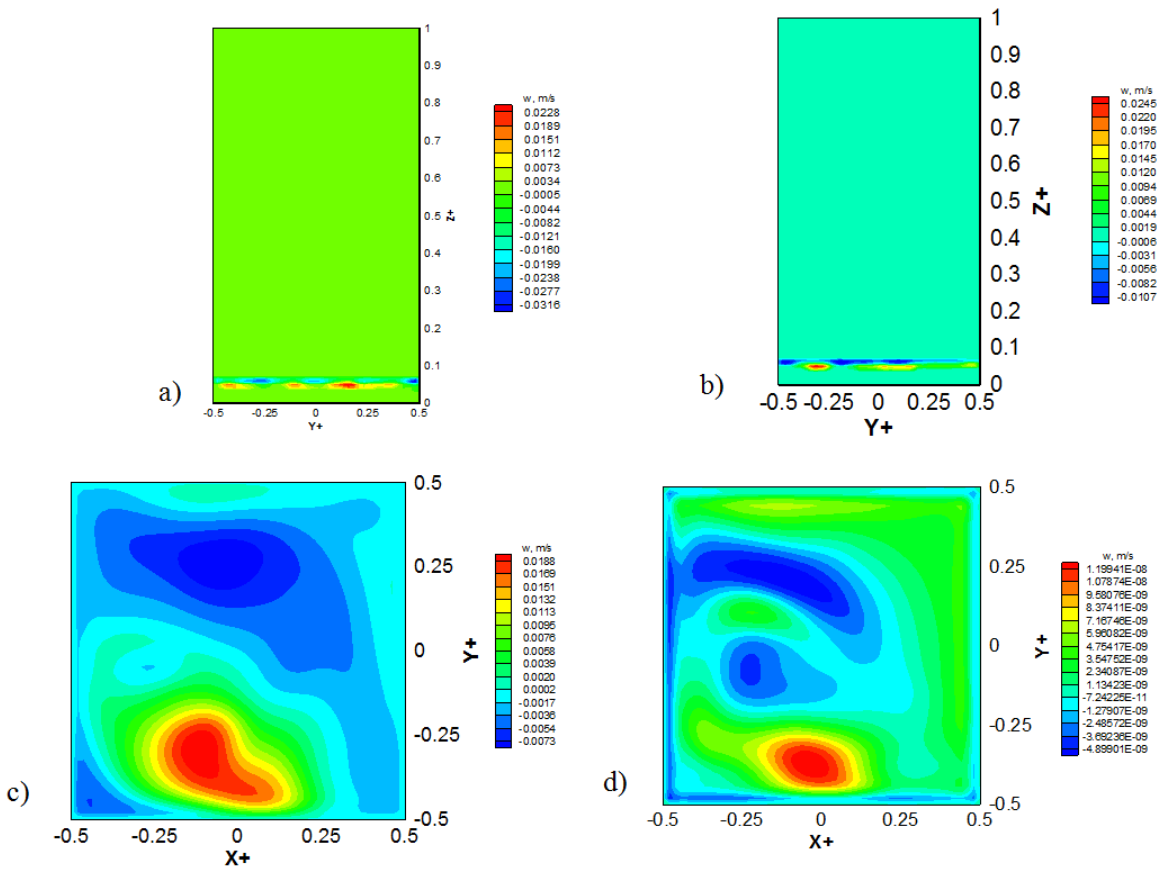

Figure 8. *z-velocity fields obtained by numerical computation at $Gr^*=3.47\times10^9$, a) x+=- 0.5, b) x+=0.5, c) z+=0.86, d) z+=1.*

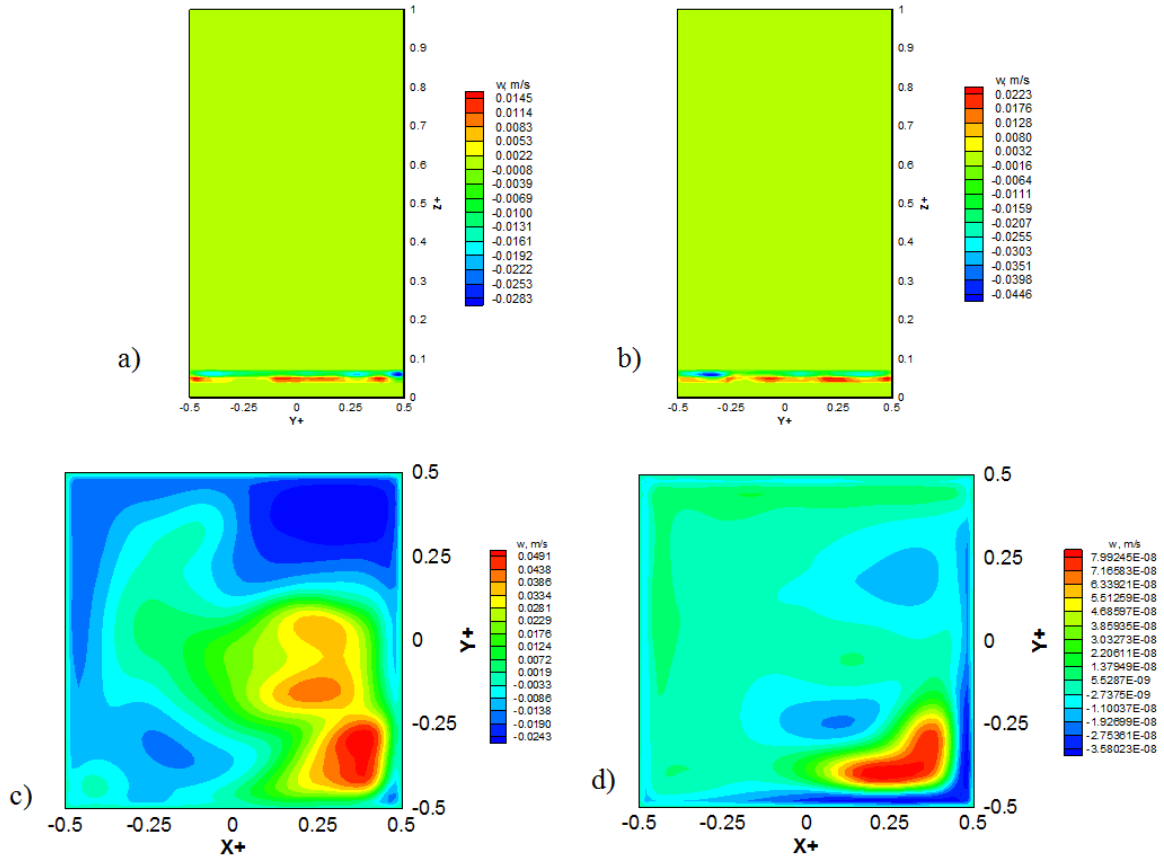

Figure 9. *z-velocity fields obtained by numerical computation at $Gr^*=4.42\times10^9$, a) x+=- 0.5, b) x+=0.5, c) z+=0.86, d) z+=1.*

4.2. Influence of Grashof Reduced Number on the z-Velocity Fields

Figure 6 represents the velocity fields obtained along the axis (0z+) at position $x+=0$ for three reduced Grashof number $Gr^*=2.1\times10^9$, $Gr^*=3.47\times10^9$ and $Gr^*=4.42\times10^9$. In Figure 6a, we observe that from the position $z+=0$ *to* 0.6 the velocity plume is almost centered and between the vertical walls and the velocity plume we observe two negative value vortices. From the position $z+=0.6$ *to* 1, the velocity values are greater than 0 m/s and almost homogeneous. In Figure 6b, we see from the position $z+=0$ *to* 0.3 the velocity plume is almost centered. From the position $z+=0.3$ *to* 1, it slopes to the left and reaches the ceiling of the enclosure where it sprawls out. The velocity plume is tilted to the right of the enclosure hits the ceiling and spreads out in Figure 6c. Between the vertical walls of the enclosure and the velocity plume, there are negative velocity zones (Figures 6b and 6c). The negative velocity recirculation zones (Figures 6a, 6b, 6c) have the effect of lowering the flow to the bottom of the enclosure.

Figures 7c, 7d, 8c, 8d, 9c and 9d show that the velocity plume reaches the ceiling of the enclosure, is destroyed and the fluid flow descends to the bottom of the enclosure. At the side walls at positions x+=-0.5 and 0.5 (Figures 7a, 7b, 8a, 8b, 9a and 9b) we see that the values of the velocityw are negative from the ceiling of the enclosure near the openings, therefore, the hot air flow descends from the ceiling downward near the openings of the enclosure. Close to the floor, the values of the velocity w are positive. So airflow rises to the top of the enclosure.

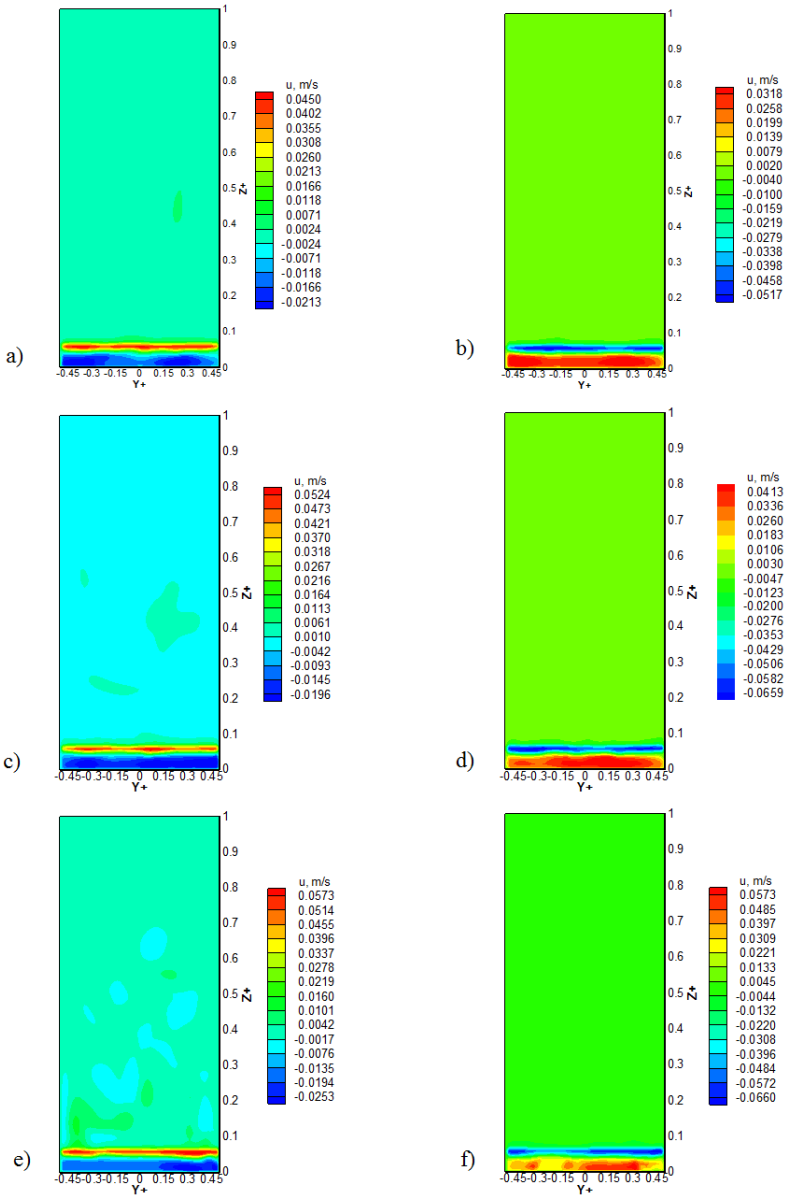

Figure 10. *x-velocity fields obtained by numerical computation a) $x+=0.5$; $Gr^*=2.1\times10^9$, b) $x+=-0.5$; $Gr^*=2.1\times10^9$, c) $x+=0.5$; $Gr^*=3.47\times10^9$, d) $x+=-0.5$; $Gr^*=3.47\times10^9$, e) $x+=0.5$; $Gr^*=4.42\times10^9$, f) $x+=-0.5$; $Gr^*=4.42\times10^9$.*

4.3. Influence of Grashof Reduced Number on the x-Velocity Fields

Figure 10 represents the velocity fields obtained along the axis (0x) and at positions x+=0.5 (right wall) and x+=*-0.5* (left wall) for three values of the reduced Grashof number $Gr^*=2.1\times10^9$, $Gr^*=3.47\times10^9$ and $Gr^*=4.42\times10^9$. It can be seen that outside the openings the velocity values are zero. The air enters the enclosure through the openings located near the floor and leaves through the openings located near the plane *z+=0.07*.

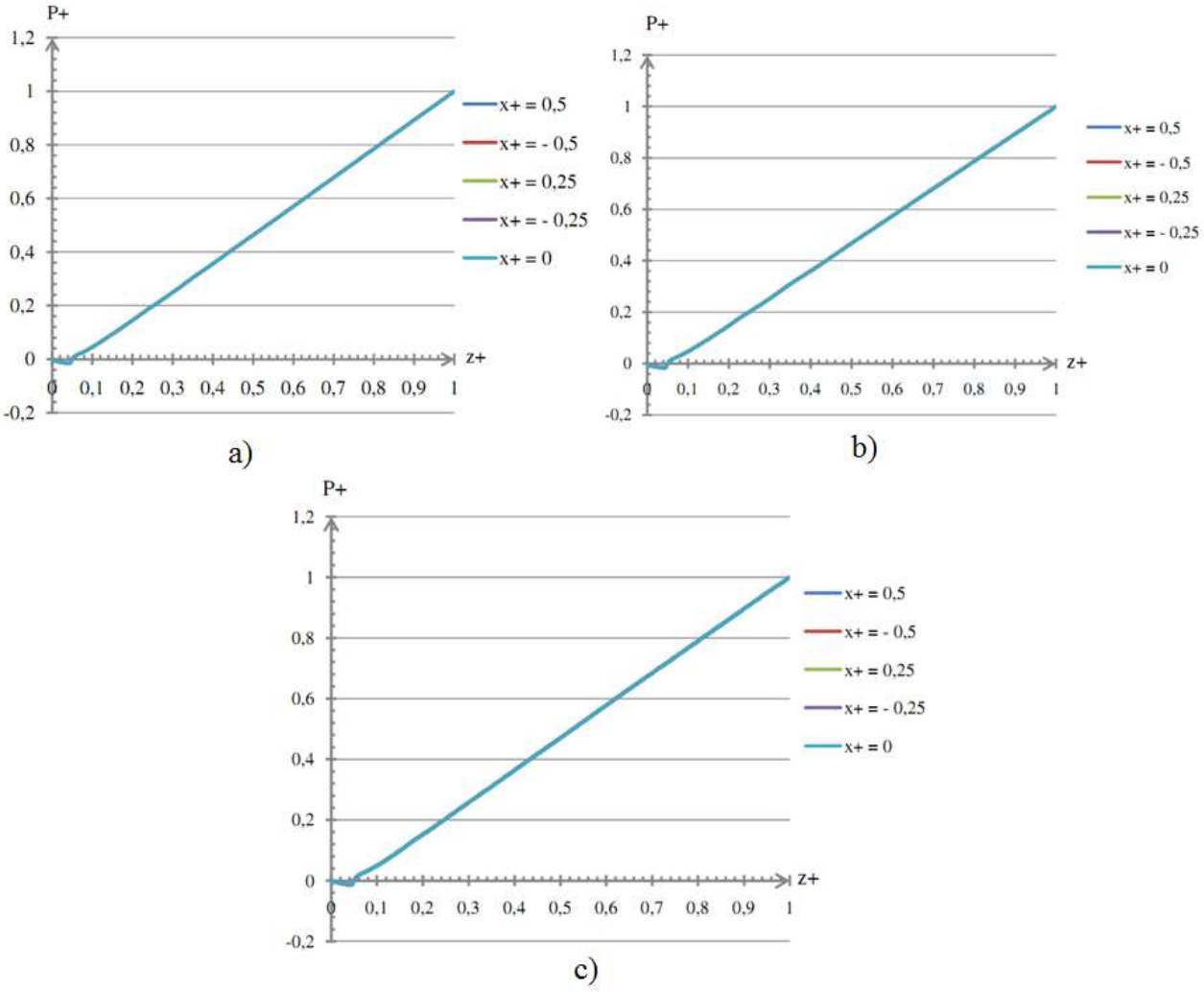

Figure 11. *Dimensionless differential pressure static vertical numerical profiles at y+=0, a) $Gr^*=2.1\times10^9$, b) $Gr^*=3.47\times10^9$, c) $Gr^*=4.42\times10^9$.*

4.4. Influence of Grashof Reduced Number on the Differential Static Pressure Profiles in Enclosure and Near the Openings

Figure 11 represents the vertical profiles of differential static pressure obtained at positions *x+=- 0.5, - 0.25, 0: 0.25, 0.5* and *y+=0* and for three values of the reduced Grashof number $Gr^*=2.1\times10^9$, $Gr^*=3.47\times10^9$ and $Gr^*=4.42\times10^9$. It can be seen that the static pressure differential profiles are almost homogeneous in the enclosure. Static pressure differential (ΔP_{stat}) values increase as the reduced Grashof number increases. For $z+ < 0.55$, $\Delta P_{stat} < 0\ Pa$. Therefore air enters the enclosure through the openings located near the floor. From the position $z+=0.55$ *to 1*, $\Delta P_{stat} \geq 0\ Pa$. This implies that hot air leaves the chamber through the openings located near the plane *z+=0.07*.

*4.5. Comparison of Differential Static Pressure Profiles en Fonction du Nombre de Raleigh Réduit Gr**

Figure 12 represents the comparison of the vertical profiles of differential static pressure obtained at positions *x+=0* and *y+=0* and as a function of three reduced Grashof number values $Gr^*=2.1\times10^9$, $Gr^*=3.47\times10^9$, $Gr^*=4.42\times10^9$. One notes from the position *z+=0 to 0.058* (Figure 12) the absolute values of differential static pressure profile are low and almost identical. From the position *z+=0.058 to 1*, the differential static pressure values increase as the reduced Grashof number (*Gr**) increases (Figure 12a). The neutral height is almost identical with the increase in *Gr** and at the value *z+=0.05* (Figure 12b).

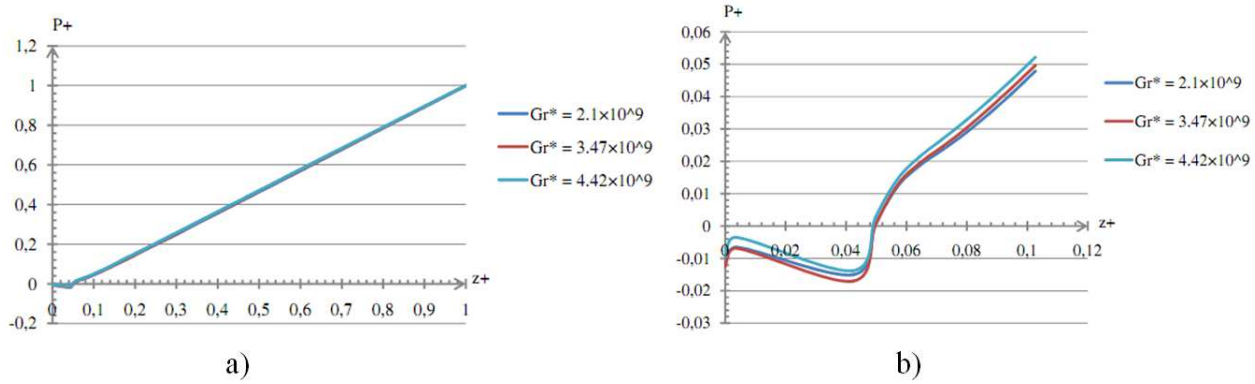

Figure 12. *Comparison of dimensionless differential pressure static vertical numerical profiles at x+=0 and y+=0 as a function of the reduced Raleigh number Gr* a) z+=0 à 1, b) z+=0 à 0.1.*

4.6. Comparison of Static Pressure Profiles Obtained by Numerical Computations with Experimental Measu-rements and Numerical Computations of Case 11

Figure 13 represents the comparison of the vertical profiles of differential static pressure obtained by numerical computation with the experimental results and numerical computations of case 11 of Koueni Toko [6] at positions *x +=0* and *y +=0*. In case 11 of the work of Kouéni Toko [6], the height of the openings located at the bottom of the enclosure is 34 mm. In this study, the height of the openings is 4 mm. Table 3 shows that the values of the maximum differential static pressure of our study are higher than that of Kouéni Toko [6]. In addition from Figure 13, we observe that the results of our study agree with the results of case 11 of Koueni Toko [6].

This difference in values of maximum differential static pressure between our study and that of KouéniToko [6] is perhaps due to the values of the temperature in the enclosure which are higher in our field of study [7] than that of Kouéni Toko [6]. And the flow of fresh air entering the enclosure, which is high (neutral height close to 0.76 h) compared to the work of Kouéni Toko [6] (neutral height close to 0.5 h).

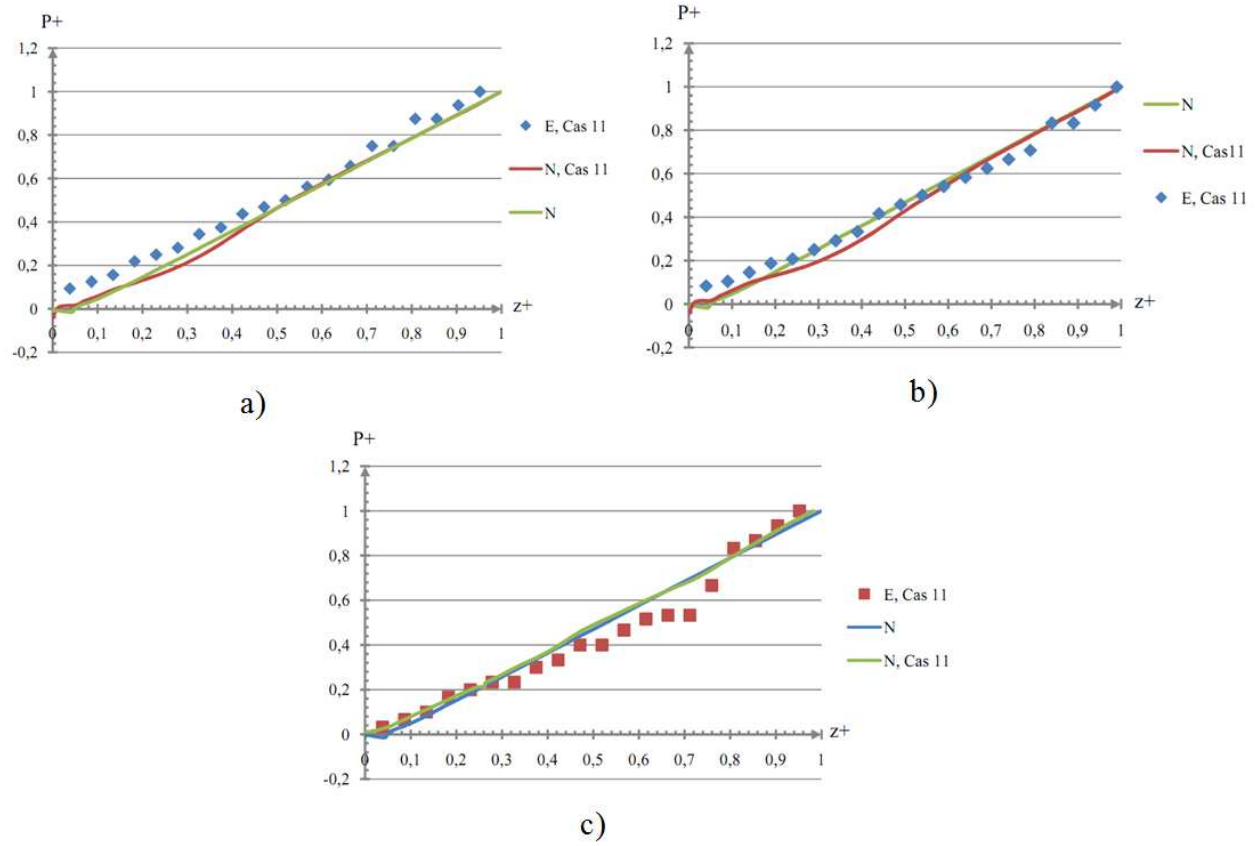

Figure 13. *Comparison of dimensionless differential pressure static vertical numerical profiles with the case 11 of experimental and numerical results Koueni Toko [6] at x+=0 and y+=0, a) Gr*=2.1×10^9, b) Gr*=3.47×10^9, c) Gr*=4.42×10^9.*

5. Conclusion

At the end of our study, it was a question of numerically studying the speed fields generated by a plume in a semi-ventilated enclosure. The enclosure under study has 20 openings located near the floor on two opposite side walls, parallel to the side section of the heat source and symmetrical with respect to the (0z) axis. Each side wall has ten openings placed in two horizontal rows in the direction (0y). The enclosure aspect ratio is 2.476. The plume is created by a linear heat source. The study is carried out in a steady state. To solve the mass and momentum conservation equations, the Direct Numerical Simulation (DNS) method and the finite volume method were used to discretize the differential equations. The fine non-uniformregular mesh was chosen to reduce calculation errors, to have a rapid convergence of the conservation equations and a stable result which approaches reality. The results obtained show that the velocity plume can have three positions in the enclosure depending on the increase in the number of reduced grashof. It can be either quasi-centered (Figures 5a and 6a) or either strongly tilted to the left of the enclosure (Figures 5c and 6c) or slightly tilted to the right (Figures 5b and 6b). The velocity plume reaches the ceiling of the enclosure where it is destroyed (Figures 7c, 7d, 8c, 8d, 9c and 9d). Near the ceiling, the velocity values w are almost zero. In the plume, the values of the velocity w are positive and there are strong velocity gradients. Between the w velocity plume and the side walls there are negative velocity recirculation zones (Figure 6) with strong velocity gradient and negative velocity values w which have the effect of lowering the air flow towards the bottom of the enclosure (Figures 7a, 7b, 8a, 8b, 9a and 9b). The air flow on the left and right side walls is at a negative velocity value w. The maximum absolute values of the velocity w in the plume and u at the openings increase with the increase in the reduced Grashof number. The neutral height is $z+=0.05$and is almost constant with increasing number of reduced Grashof. The maximum value of the static pressure differential increases as the number of reduced Grashof increases. Below the neutral height the values of the static pressure differential are negative and positive above.

In the case of Koueni Toko [6], cool air enters and hot gases exit the enclosure at each of the openings. The determinations of the neutral height and the mass flow rates entering and leaving the enclosure are complex. With the help of our study this problem is solved through the multiple openings located at the bottom of the enclosure. The neutral height is 0.76 of the height h=34 mm (Figure 12b) therefore, the cool air enters the enclosure through the openings located near the floor and the hot gases exit the enclosure through the localized openings. In the neighborhood of h (Figure 10).

The comparison of the dimensionless static pressure differential profiles obtained with the experimental results and numerical calculations of case 11 of Koueni Toko [6] is consistent.

In perspective, numerical calculations of the velocity fields can be performed in unsteady state to better understand the phenomenon of hot air filling in the enclosure.

Nomenclature

Lowercase

l	Width Enclosure, m
x	Longitudinal coordinate, m
y	Vertical coordinate, m
z	Transverse coordinate, m
u	Horizontal component of the velocity, $m.s^{-1}$
v	Vertical component of the velocity, $m.s^{-1}$
w	Transverse velocity component, $m.s^{-1}$
cte	Constant
h_i	Heat exchange coefficient inside the enclosure, $W.m^{-1}.K^{-1}$
h_o	Heat exchange coefficient outside the enclosure, $W.m^{-1}.K^{-1}$

Capital Letters

L	Enclosure length, m
H	Enclosure height, m
ΔT_0	Temperature difference between the heat source and the outside, K
T	Temperature inside the enclosure, K
T_0	Temperature of the heat source, K
U_0	Maximum inlet gas velocity in the enclosure, K
P	Static pressure inside enclosure, Pa
P_{max}	Maximum static pressure inside enclosure, Pa
P_{total}	Total pressure, Pa
$P_{total,\ inside}$	Total pressure inside the enclosure, Pa
$P_{total,outside}$	Total pressure outside the enclosure, Pa
$T_{outside}$	Temperature outside the enclosure, K
T_p	Side wall or ceiling temperature, K
T_∞	Temperature away from side wall or ceiling inside or outside the enclosure, K
S_1	Section of the enclosure ceiling, m^2
S_2	Section of the side walls of the enclosure, m^2

Greek Symbols

ν	Kinematic viscosity of air, $m^2.s^{-1}$
ρ	Density, $kg.m^{-3}$
β	Coefficient of thermal expansion, K^{-1}
ρ_{ext}	Density of gases outside of the enclosure, $kg.m^{-3}$
φ_p	Heat flux to the side walls and ceiling of the enclosure, $W.m^{-1}$
λ	Thermal conductivity of the walls in Plexiglas, $W.m^{-1}.K^{-1}$

Dimensionless Numbers

Pr	Prandtl number
Gr	Grashof number

Special Characters

Gr*	Reduced Grashof number
x+	Dimensionless longitudinal coordinate
y+	Dimensionless vertical coordinate
z+	Coordinated transverse to size
u+	Horizontal component of the dimensionless speed
v+	Vertical component of the dimensionless speed
w+	Transverse component of the dimensionless speed
P+	Static pressure to size
T+	Temperature to size
δ	Aspect Ratio

References

[1] Morton B. R., Geoffrey Taylor, Turner J. S. (1956) Turbulent Gravitational Convection from Maintained and Instantaneous Sources, *Proceedings of the Royal Society of London. Series A, Mathematical and Physical Sciences,* 234 N° 1196, 1-23.

[2] Auban O., Lemoine F., Valette P., Fontaine J. R. (2001) Simulation by solutal convection of a thermal plume in a confined stratified environment: application to displacement ventilation, *International Journal of Heat and Mass Transfer*, 44, 4679-4691.

[3] Baines W. D., Turner J. S. (1969) Turbulent buoyant convection from a source in a confined region, *Journal of Fluid Mechanics*, 37, 51-80.

[4] Grae Worster M., Leitch Alison M. (1985) Laminar free convection in confined regions, *Journal of Fluid Mechanics,* 156, 301-319.

[5] Chow W. K., Cui E., Li Y. Z., Huo R., Zhou J. J. (2000) Experimental Studies on Natural Smoke Filling in Atria, *Journal of Fire Sciences,* vol. 18, 84-103.

[6] Koueni Toko C. A. (2019) Etude des champs dynamique et thermique dans une enceinte semi-ventilée en convection naturelle, *Rapportannuel dethèse-CORIA.*

[7] Kouéni–Toko C. A., Tcheukam–Toko D., Kuitche A., Patte-Rouland B., Paranthoën P. (2021) Numerical modeling of the temperature fields in a semi-confined enclosure heated by a linear heat source, *International Journal of Thermo fluids,* Vol. 7-8, 100017.

[8] Fitzgerald S. D. and Woods A. W. (2010) Transient natural ventilation of a space with localized heating, *Building and Environment*, 45 2778-2789.

[9] Jeremy C. P. and Andrew W. W. (2004), On ventilation of a heated room through a single doorway, *Building and Environment,* 39 241-253.

[10] Paranthoën P. and Gonzalez M. (2010), Mixed convection in a ventilated enclosure, *International Journal of Heat and Fluid Flow,* 31 172-178.

[11] Linden P. F., Lane-Serff G. F., Smeed D. A. (1990) Emptying filling boxes: the fluid mechanics of natural ventilation, *Journal of Fluid Mechanics*, 212, 309–335.

[12] Kaye N. B. and Hunt G. R. (2004) Time-dependent flows in an emptying filling box, *Journal of Fluid Mechanics,* 520, 135-156.

[13] Gladstone C. and Woods A. W. (2001) On buoyancy-driven natural ventilation of a room with a heated floor, *Journal of Fluid Mechanics*, 441, 293-314.

[14] Kaye N. B., Hunt G. R. (2007) Overturning in a filling box, *Journal of Fluid Mechanics*, 576, 297-323.

[15] Karl Terpager Andersen (2003) Theory for natural ventilation by thermal buoyancy in one zone with uniform temperature, *Building and Environment*, 38, 1281-1289.

[16] Patankar S. V. (1980) Numerical heat transfert and fluid flow, *Hemisphere Publishing Corporation.*

[17] Leonard, B. P. (1979) A stable and accurate convective modeling procedure based on quadratic interpolation, *Comput methods Appl. Mech. Eng.,* 19, 59-98.